

# Assessment of bed macrostructuring and thermal wave impact on carbon dioxide adsorption efficiency in a hybrid fixed-bed reactor

Marcin Gunia<sup>1</sup>, Julia Ciećko<sup>1</sup>, Katarzyna Bizon\*<sup>1</sup>

Faculty of Chemical Engineering and Technology, Cracow University of Technology, Warszawska 24, 31-155 Kraków, Poland

## \* Corresponding author:

e-mail:

[katarzyna.bizon@pk.edu.pl](mailto:katarzyna.bizon@pk.edu.pl)

Presented at 24th Polish Conference of Chemical and Process Engineering, 13–16 June 2023, Szczecin, Poland.

## Article info:

Received: 28 April 2023

Revised: 09 June 2023

Accepted: 29 June 2023

## Abstract

The development of efficient carbon dioxide sequestration and utilization technologies is an indispensable aspect of a wide range of measures directed at reducing the negative effects of anthropogenic emissions on the environment. One route is its capture via physical adsorption and further conversion to methane in the Sabatier reaction. The sorption process can be carried out in fixed-bed adsorptive reactors, in which the packing is made up of adsorbent and catalyst particles. Proper structuring of such a hybrid bed can contribute to increasing the efficiency of both stages of the process. Of importance in this regard is, first of all, the proper management of heat transfer. This study examines the sorption step of the operation of an adsorptive reactor for CO<sub>2</sub> sequestration and methanation using a one-dimensional non-isothermal model of a layered fixed bed. Numerical calculations for different configurations and different volume adsorbent to catalyst ratios were carried out to determine how the hybrid structure of the bed and the atypical thermal waves it induces affect the sorption process. The results obtained prove that proper tailoring of the bed can be an excellent tool to control the temperature profiles and thus the performance of the apparatus and possibly its optimization.

## Keywords

hybrid fixed bed, CO<sub>2</sub> sequestration, adsorptive reactor, mathematical modelling

## 1. INTRODUCTION

The continuous growth of carbon dioxide concentration in the atmosphere is one of the biggest environmental concerns contributing to global warming and climate change. It can be stated that circa 77% of total greenhouse emissions constitutes CO<sub>2</sub> (Patra et al., 2022). Most of it originates from anthropogenic emissions caused by the use of fossil fuels, in refineries, chemical industry and power plants, as well as in vehicle engines and domestic heating. All this is forcing scientists to conduct intensive research to develop technologies and processes for carbon dioxide capture, and possibly its further utilization. Such technologies would allow to reduce the carbon dioxide concentration in the atmosphere, making it possible to fulfill the plan to limit the global warming temperature to 1.5 °C (Masson-Delmotte et al., 2018). Among these processes there is especially growing interest in CO<sub>2</sub> capture based on post-combustion adsorption (Chao et al., 2021) and reactive adsorption (Maina et al., 2021), with the latter methodology in particular likely to be a promising alternative in gas separation. Such processes attract the attention of researchers mainly because of their flexibility, namely, adsorption columns can be coupled with existing industrial facilities that operate under different conditions.

Generally, there are two different options to further manage the captured CO<sub>2</sub>: it is possible to store it (then it is referred to as carbon capture and storage – CCS) or to further utilize it (carbon capture and utilization – CCU), sometimes

the latter technology is termed CCUS, standing for carbon capture utilization and sequestration (Patra et al., 2022). Carbon dioxide is separated from the flue gases, exhaust gases or directly from the ambient air through, for example, adsorption, absorption or membrane processes, and in next step the carbon dioxide free gas is released while CO<sub>2</sub> can be further utilized, for example, in the synthesis of synthetic fuels. Reutilization of carbon dioxide implies that it is no longer viewed as waste, but a valuable chemical compound that has been given a “second life” (Styring et al., 2021). In fact, the separation process can be combined with a chemical reaction, specifically the reactive regeneration of a saturated sorbent bed that follows periodically (in the case of fixed-bed columns) the adsorption (sequestration) process. For example, carbon dioxide can react with gaseous hydrogen in a methanation reaction to produce methane (Jo et al., 2022; Miguel et al., 2017), or it is possible to go further and convert it into methanol (Hira et al., 2023). Catalytic hydrogenation of CO<sub>2</sub> to methane via the Sabatier reaction can be interfaced with the exploitation of excess renewable energy converted to hydrogen in electrolysis. Such process integration falls within the framework of the technologies that are now being developed intensively named power-to-gas or more generally power-to-X and aimed at achieving net-zero emissions (Hira et al., 2023). It also falls within the broad concept of integration and intensification of chemical processes, which represent the core of modern chemical engineering and are among the main instruments towards energy transition (Moioli, 2022).



When an adsorptive reactor is chosen for separation of CO<sub>2</sub>, in which the sorbent integrated in this case with catalyst particles is reactively regenerated, the process can be classified as sorption-enhanced reaction process (SERP). Typically, this term refers to reactors in which one of the by-products is selectively removed from the reaction environment by adsorption, anyhow, in SERP an adsorbent can be also exploited as a source for reacting species (Agar, 2005), in the case of Sabatier reaction it is CO<sub>2</sub>. SERPs are a good alternative to conventional processes in which separation and reaction take place in two separate apparatuses.

Turning the focus on carbon dioxide capture by adsorption in an adsorptive reactor, which is currently receiving a lot of attention in the scientific community, it is apparent that there are many ways of conducting this process, starting from different reactor types, through different sorbent regeneration modes (Dhoke et al., 2021), to different modalities of integration of various types of sorbents, e.g. zeolites or hydrotalcite (Choi et al., 2003; Ding and Alpay, 2000), and catalysts, e.g. nickel, ruthenium (Bremer et al., 2017; Moiola and Z utzel, 2020), within the bed. Among the reactors suitable for conducting this process, there are fixed-bed, moving-bed and fluidized-bed reactors. The right contact of the phases is crucial to achieve the best economic results of the process. The fixed bed is the simplest option, enabling the use of structured packing, and thus making it possible to optimize the size of the contact area. The main drawback of this type of apparatus is the occurrence of high pressure drops and the cyclic nature of the operation. Alternatively, a moving or fluidized-bed reactor can be used, which, unlike the fixed bed version, allows continuous operation. However, the use of a bed composed of moving particles introduces additional complexity in the design and operation of the system (Dhoke et al., 2021).

Given that fixed-bed adsorption columns typically operate under non-isothermal conditions, due to the exothermic nature of the adsorption process, proper heat transfer management is necessary. It is well known that when adsorbate is introduced into the column, a thermal wave is generated that propagates through the bed. Its shape and advancement depend principally on the adsorptive, thermal and transport properties of the system and the gas flow rate (Kagueli et al., 1989; Martins et al., 2022; Pan and Basmaadjian, 1970). This phenomenon should be taken into account, especially in the case of a feed with a rather high concentration of adsorbate (i.e. from a few to over a dozen percent by volume), when a large amount of gas is adsorbed and therefore a significant amount of heat is generated, or for adsorbate-adsorbent systems characterized by relatively high values of isosteric heat of adsorption. For example, for zeolite-based adsorbents, the value of the isosteric heat of adsorption of carbon dioxide can range from about 20 kJ/mol to even more than 50 kJ/mol (Harlick and Tezel, 2004; Thang et al., 2014). Several ways of managing the released heat are known, the most well-known being the in-bed heat exchangers and materials which can

store a large amount of heat and can be mixed with the adsorbent (Rezaei and Grahn, 2012; Rezaei and Webley, 2009). Another possible solution for adsorption columns is a layered bed, where the adsorbent layer (or layers) is followed by an inert layer (or layers). In the case of adsorptive reactors, this function is performed by catalyst particles, which can be sandwiched in layers between the adsorbent particles or mixed with them. In such a configuration, the inert (catalyst) acts as a "coolant" as it absorbs the heat released during the adsorption process from the flowing gas. This configuration prevents the formation of local hotspots (Hussainy and Agar, 2018), which cause unwanted desorption of the already captured substance. In adsorptive reactors, instead of a layered bed or a bed composed of a physical mixture of adsorbent and catalyst particles, more innovative solutions can be implemented, such as dual-function materials (DFM) containing both adsorbent and catalyst functionalities (Martins et al., 2022; Miguel et al., 2017).

It is expected that the appropriate spatial arrangement of various bed functionalities in the reactor with alternating layers of adsorbent and catalyst ("sandwich" type bed) can lead to better heat management and more efficient operation of this apparatus. However, there are no literature reports in this regard. Therefore, this study examined the operation of an adsorptive reactor for CO<sub>2</sub> sequestration and methanation. Due to the complexity of the process, the focus at this stage was on the adsorption step. Numerical studies were carried out with the use of a one-dimensional non-isothermal model of a layered bed. The performance of the hybrid fixed bed for different configurations and different volume ratios of adsorbent and catalyst (treated here as inert) was assessed based on bed breakthrough times and the amount of carbon dioxide adsorbed within that time.

## 2. MATHEMATICAL MODEL AND SOLUTION METHODOLOGY

### 2.1. Governing equations

The analysis was conducted using a one-dimensional model of a fixed-bed adsorptive reactor with the bed consisting of alternating layers of adsorbent and catalyst particles, where the latter is treated as inert during the adsorption stage. In addition, for comparative purposes, calculations were performed for a bed consisting of a uniform physical mixture of adsorbent and catalyst particles (Fig. 1).

In light of previous studies (Al-Janabi et al., 2018; Choi et al., 2003; Ko et al., 2003; Raghavan and Ruthven, 1984) and considering the main purpose of this work, the following assumptions were made to formulate the mathematical model of the hybrid bed:

- the radial variation of concentration and temperature is negligible,
- the system is assumed to be adiabatic,

- the gas phase and the bed particles are in local thermal equilibrium,
- the gas mixture fed to the apparatus at the adsorption stage contains only CO<sub>2</sub> and N<sub>2</sub>,
- the inlet concentration of adsorbable component (CO<sub>2</sub>), is kept low, and thus the gas velocity is assumed to be constant throughout the bed,
- the gas follows the ideal gas law, and the pressure drop is neglected,
- the gas flow is described using the axially dispersed plug flow model,
- the adsorption equilibrium is described by the Toth isotherm and the mass transfer rate is described by a linear driving force (LDF) model,
- physical and transport properties are assumed to be independent of temperature,
- the energy balance incorporates the so-called effective thermal conductivity of the bed, which depends on the thermal conductivities of the gas and the solids, and the gas velocity.

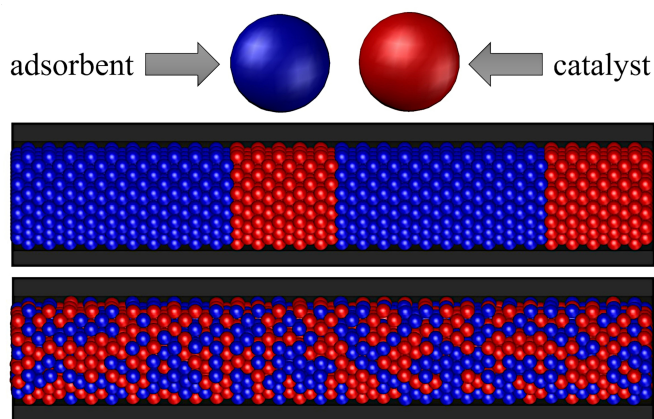


Figure 1. Scheme of the experimental setup: 1 – air compressor; 2 – pressure regulator; 3 – mass flow controller; 4 – thermostat; 5, 6, 7, and 8 – scrubbers with VOCs; 9a – inlet sampling point; 9b – outlet sampling point; 10 – fixed bed adsorber with the inside diameter of 3.2 cm (Jurkiewicz et al., 2023)

Both the constant velocity assumption and the omission of pressure drop are motivated by the conditions adopted in the calculations and the conclusions of previous work by other authors. As demonstrated by Al-Janabi et al. (2018) who studied the effect of velocity variation when modelling CO<sub>2</sub> adsorption in fixed beds, it is important to consider velocity variation when the adsorbate concentration in the feed is significant. Nevertheless, for the low concentration values considered in this study, the deviation of the breakthrough time obtained under the assumption of constant velocity from that determined using the model taking into account its variation due to adsorption is of the order of 1% (Al-Janabi et al., 2018). Also, the pressure drop along the bed, calculated here from Ergun's equation for the physical and geometric, and process parameters values assumed in the numerical sim-

ulations, does not exceed 1% of the pressure at the inlet. The assumption that the only component subject to adsorption is CO<sub>2</sub> is justified by the findings reported in the Reference (Shigaki et al., 2020). The authors demonstrated that due to the much higher adsorption affinity of zeolite 13X towards CO<sub>2</sub> than N<sub>2</sub>, the presence of nitrogen in the mixture has no significant effect on the equilibrium amount of adsorbed carbon dioxide compared to the case of single component adsorption.

Given the aforementioned assumptions, the mass balance of CO<sub>2</sub> in the gas phase can be written as follows:

$$(\varepsilon_{t,ads} f_{ads} + \varepsilon_{t,cat} f_{cat}) \frac{\partial C_{CO_2}}{\partial t} = \varepsilon_b D_{ax} \frac{\partial^2 C_{CO_2}}{\partial x^2} - u \frac{\partial C_{CO_2}}{\partial x} - \rho_{b,ads} f_{ads} \frac{\partial q_{CO_2}}{\partial t} \quad (1)$$

with the mass transfer in the solid phase described by the linear driving force (LDF) model:

$$\frac{\partial q_{CO_2}}{\partial t} = k (q_{CO_2}^* - q_{CO_2}) \quad (2)$$

where:

$$k = \frac{15D_e}{r_p^2} \quad \text{and} \quad D_e = \frac{\varepsilon_p D_K \cdot D_m}{\tau_p D_K + D_m} \quad (3)$$

In Eq. (1)  $f_{ads}$  and  $f_{cat} = 1 - f_{ads}$  denote, respectively, the volume fraction of adsorbent and catalyst particles being functions of longitudinal coordinate in the reactor,  $x$ . The symbol  $\varepsilon_t$  denotes the total voidage of the bed accounting both for inter-particle voids and particle pores, i.e.  $(1 - \varepsilon_t) = (1 - \varepsilon_b)(1 - \varepsilon_p)$ .

The equilibrium concentration,  $q_{CO_2}^*$ , in the solid phase was described by the Toth isotherm for zeolite 13X (Wang and LeVan, 2009):

$$q_{CO_2}^* = \frac{a p_{CO_2}}{[1 + (b p_{CO_2})^\tau]^{1/\tau}} \quad (4)$$

where:

$$a = a_0 \exp\left(\frac{E}{T}\right), \quad b = b_0 \exp\left(\frac{E}{T}\right) \quad \text{and} \quad \tau = \tau_0 + \frac{c}{T} \quad (5)$$

The axial dispersion coefficient,  $D_{ax}$ , was calculated using the following expression proposed by Wakao and Funazkri (1978):

$$D_{ax} = \frac{D_m}{\varepsilon_b} (20 + 0.5 Sc Re_p) \quad (6)$$

The viscosity of the gas mixture was calculated using Wilke's formula (Poling et al., 2001). Given the binary nature of the mixture and ideal gas conditions, the molecular diffusion coefficient,  $D_m$ , was determined from the formula proposed independently by Chapman and Enskog (Poling et al., 2001). The effective diffusion coefficient,  $D_e$ , defined in Eq. (3) accounts both for molecular and Knudsen diffusion, with the

coefficient of the latter calculated using a classical formula that originates from the kinetic theory of gases (Do, 1998).

The energy balance for the gas and solid phases inside the column is expressed by the following equation:

$$\begin{aligned} & [(\varepsilon_{t,ads}f_{ads} + \varepsilon_{t,cat}f_{cat})\rho_g c_g \\ & + \rho_{b,ads}f_{ads}(c_{s,ads} + c_{ads}) + \rho_{b,cat}f_{cat}c_{s,cat}] \frac{\partial T}{\partial t} \\ & = K_{ax} \frac{\partial^2 T}{\partial x^2} - u\rho_g c_g \frac{\partial T}{\partial x} + \rho_{b,ads}f_{ads}(-\Delta H_{ads}) \frac{\partial q_{CO_2}}{\partial t} \end{aligned} \quad (7)$$

For the sake of simplicity, constant average values of  $\rho_g$  and  $c_g$  were adopted in the calculations. The same applies to the adsorbed phase heat capacity,  $c_{ads}$ , and the enthalpy of adsorption,  $\Delta H_{ads}$ , with the latter determined using the Clausius–Clapeyron equation (Do, 1998):

$$\begin{aligned} -\Delta H_{ads} &= \frac{RT^2}{p_{CO_2}} \left( \frac{\partial p_{CO_2}}{\partial T} \right)_{q_{CO_2}^*} \quad \text{where} \\ p_{CO_2} &= \frac{q_{CO_2}^*}{[a\tau - (q_{CO_2}^* b)^\tau]^{1/\tau}} \end{aligned} \quad (8)$$

The effective thermal conductivity,  $K_{ax}$ , was calculated using the formula accounting for solid, stagnant (film) and flowing gas contributions (Kunii and Smith, 1960; Yagi et al., 1960):

$$K_{ax} = K_{ax}^0 + \lambda_g a \text{Pr} \text{Re}_p \quad (9)$$

where:

$$\begin{aligned} K_{ax}^0 &= \lambda_g \varepsilon_b + \lambda_g \frac{\beta(1 - \varepsilon_b)}{\psi_t + \gamma/\kappa} \\ \kappa &= \frac{\lambda_s}{\lambda_g} \quad \text{and} \quad a = 0.5 \end{aligned} \quad (10)$$

and:

$$\begin{aligned} \psi_t &= \psi_2 + (\psi_1 - \psi_2) \frac{\varepsilon_b - 0.260}{0.216} \\ \text{for } 0.260 &\leq \varepsilon_b \leq 0.476 \end{aligned} \quad (11)$$

$$\psi_j = \frac{1}{2} \frac{\left( \frac{\kappa - 1}{\kappa} \right)^2 \sin^2 \theta_j}{\ln [\kappa - (\kappa - 1) \cos \theta_j] - \frac{\kappa - 1}{\kappa} (1 - \cos \theta_j)} - \frac{2}{3\kappa} \quad (12)$$

for  $j = 1, 2$ ,

$$\sin^2 \theta_j = \frac{1}{n_j} \quad \text{where } n_1 = 1.5 \quad \text{and} \quad n_2 = 4\sqrt{3} \quad (13)$$

The thermal conductivity of gas mixture appearing in Eq. (9) and (10) was determined by means of Wassiljewa equation (Poling et al., 2001). Values  $n_j$ ,  $j = 1, 2$ , in Eq. (13) represent a number of contact points on a semi-spherical surface of one solid particle within the bed, with  $n_1$  and  $n_2$ , referring to loose ( $\varepsilon_b = 0.476$ ) and close packing ( $\varepsilon_b = 0.260$ ), respectively.

To solve the system of partial differential equations describing the dynamics of the bed (Eq. (1) and Eq. (7)) coupled

with the LDF model (Eq. (2)), the model equations have to be supplemented with boundary and initial conditions. The boundary conditions for the adsorption step are defined here as follows:

$$-D_{ax} \frac{\partial C_{CO_2}}{\partial x} = \frac{u}{\varepsilon_b} (C_{f,CO_2} - C_{CO_2}) \quad \text{at } x = 0 \quad \text{and} \quad (14)$$

$$\frac{\partial C_{CO_2}}{\partial x} = 0 \quad \text{at } x = L$$

$$-K_{ax} \frac{\partial T}{\partial x} = u\rho_g c_g (T_f - T) \quad \text{at } x = 0 \quad \text{and} \quad (15)$$

$$\frac{\partial T}{\partial x} = 0 \quad \text{at } x = L$$

while the initial conditions, assuming that the bed is initially filled with inert gas, are:

$$\begin{aligned} C_{CO_2}(x, 0) &= q_{CO_2}(x, 0) = 0, \\ T(x, 0) &= T_0 \quad \text{for } 0 \leq x \leq L \end{aligned} \quad (16)$$

## 2.2. Model parameters and numerical methods employed

The model equations (Eqs. (1)–(2) and Eq. (7)) with associated boundary (Eqs. (14)–(15)) and initial (Eq. (16)) conditions were solved numerically using the method of lines, which consists in approximating the spatial derivatives using finite differences, followed by integrating in time the resulting semi-discrete system of ordinary differential equations. Particularly, in this study the spatial domain was discretized using  $N = 251$  equidistant nodes. Given the variable properties of the layered bed and the presence of the source term in the model equations only when  $f_{ads}(x)$ , i.e. the volume fraction of adsorbent particles in the bed, is non-zero, the selection of 251 grid nodes was preceded by a convergence analysis. Moreover, to avoid discontinuities in bed properties when sandwiching adsorbent and catalyst, and in effect numerical challenges,  $f_{ads}(x)$  was described by the following combination of double sigmoid functions:

$$\begin{aligned} f_{ads}(x) &= 1 - \sum_{i=1}^{M/2-1} \frac{1}{1 + \exp[-A(x - x_{2i-1})]} \\ &\cdot \frac{1}{1 + \exp[A(x - x_{2i})]} - \frac{1}{1 + \exp[-A(x - x_{M-1})]} \end{aligned} \quad (17)$$

where  $M$  is the total number of adsorbent and catalyst layers, and the symbols  $x_i$  represent the location coordinates of the endpoints of successive layers. Thus, for instance, for a bed with a length of  $L = 1$  m, consisting of  $M = 4$  layers and characterized by a ratio (by volume) of adsorbent to catalyst,  $ads:cat$ , equal to 2:1, one has:  $x_1 = 0.333$ ,  $x_2 = 0.5$  and  $x_3 = 0.833$  (Fig. 2a). In all simulations, the value of the sigmoid slope,  $A$ , appearing in Eq. (17) was assumed to be 1000.

The system of ordinary differential equations resulting from the model discretization was solved in Matlab software using

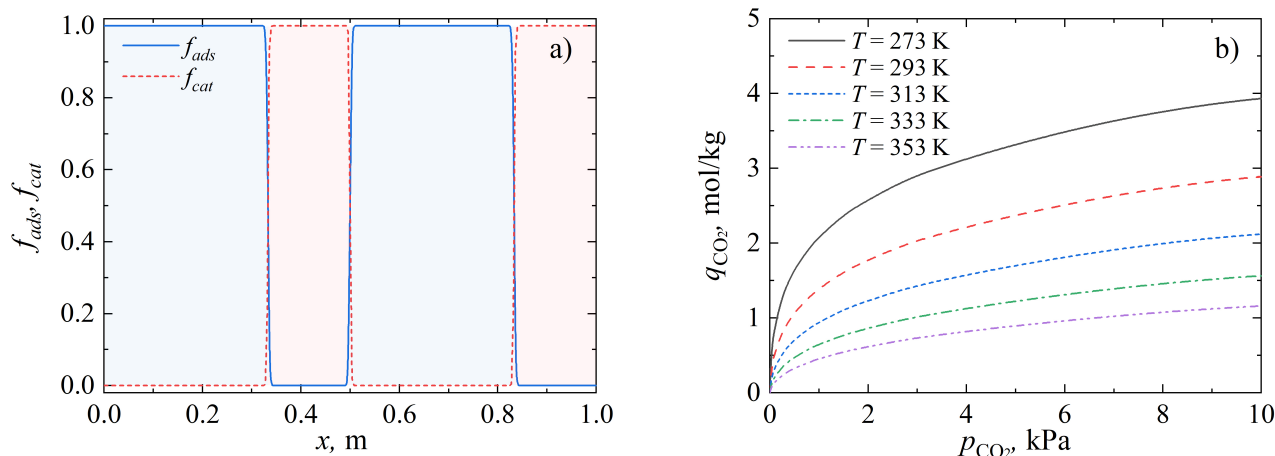


Figure 2. Distributions of adsorbent,  $f_{ads}(x)$ , and catalyst,  $f_{cat}(x)$ , fractions for  $M = 4$  and  $ads:cat = 2:1$  (a), and adsorption equilibrium isotherms of  $CO_2$  on zeolite 13X at different temperatures (b) calculated following Reference (Wang and LeVan, 2009).

the *ode23tb* solver for stiff differential equations which combines an implicit Runge–Kutta formula with a trapezoidal rule step and a backward differentiation formula. Simulations were conducted until the bed breakthrough time,  $t_b$ , defined here as the instant at which  $y_{CO_2,out}/y_{CO_2,in} = 0.01$ . To assess the performance of the adsorption process for different bed structures, for each case analyzed, the average solid phase concentration of carbon dioxide corresponding to the breakthrough time was calculated using the following formula:

$$Q_{CO_2} = \frac{1}{L} \int_0^L q_{CO_2}(x, t_b) dx \quad (18)$$

As anticipated in the previous section, simulation studies were carried out for a fixed bed consisting of alternating layers of adsorbent and catalyst particles (treated as inert during adsorption) and for a bed consisting of a uniform physical mixture of both types of particles. In the first case, calculations were made for the bed composed of  $M = 2, 4, 6, 8$  and 10 total layers. For both sandwich-like arrangement and physical mixture of particles the volume ratio of adsorbent to catalyst particles,  $ads:cat$ , was varied from 2:1 to 6:1.

The main parameter values employed in the numerical simulations are given in Table 1. Particularly, the parameters of Toth's model (Eqs. (4) and (5)) were adapted from the work of Wang and LeVan (2009), who experimentally studied the adsorption of carbon dioxide and water vapor on zeolites 13X and 5A. The resulting adsorption isotherms of  $CO_2$  on zeolite 13X employed in this study are shown in Fig. 2b. The physical parameters of the catalyst, treated as inert in the adsorption step, represent nickel catalyst (Bremer et al., 2017).

### 3. RESULTS AND DISCUSSION

#### 3.1. Evaluation of the global performance of the hybrid fixed bed

The impact of process parameters and bed structure on the global efficiency of the adsorption process in the hybrid bed was analyzed in the first step. Figure 3 shows the results of numerical simulations, reported here globally in terms of the breakthrough time,  $t_b$  (Fig. 3a), and the average concentration of carbon dioxide in the solid phase,  $Q_{CO_2}$  (Fig. 3b),

Table 1. Values of key parameters used in the simulations.

Parameter	Value	Parameter	Value	Parameter	Value
$c_{s,ads}$	1100 J/(kg·K)	$\epsilon_b$	0.45	$\tau_p$	3
$c_{s,cat}$	1107 J/(kg·K)	$\epsilon_{p,ads}$	0.54	$a_0$	$6.509 \cdot 10^{-3}$ mol/(kg·kPa)
$d_p$	$2 \cdot 10^{-3}$ m	$\epsilon_{p,cat}$	0.6	$b_0$	$4.884 \cdot 10^{-4}$ 1/kPa
$L$	1 m	$\rho_{p,ads}$	1085 kg/m <sup>3</sup>	$c$	$3.805 \cdot 10$ K
$p$	101325 Pa	$\rho_{p,cat}$	2355 kg/m <sup>3</sup>	$E$	$2.991 \cdot 10^3$ K
$T_0 = T_f$	300 K	$\lambda_{s,ads}$	0.15 W/(m·K)	$\tau_0$	$7.487 \cdot 10^{-2}$
$y_{CO_2,in}$	0.05	$\lambda_{s,cat}$	0.84 W/(m·K)	$-\Delta H_{ads}$	$3.898 \cdot 10^4$ J/mol

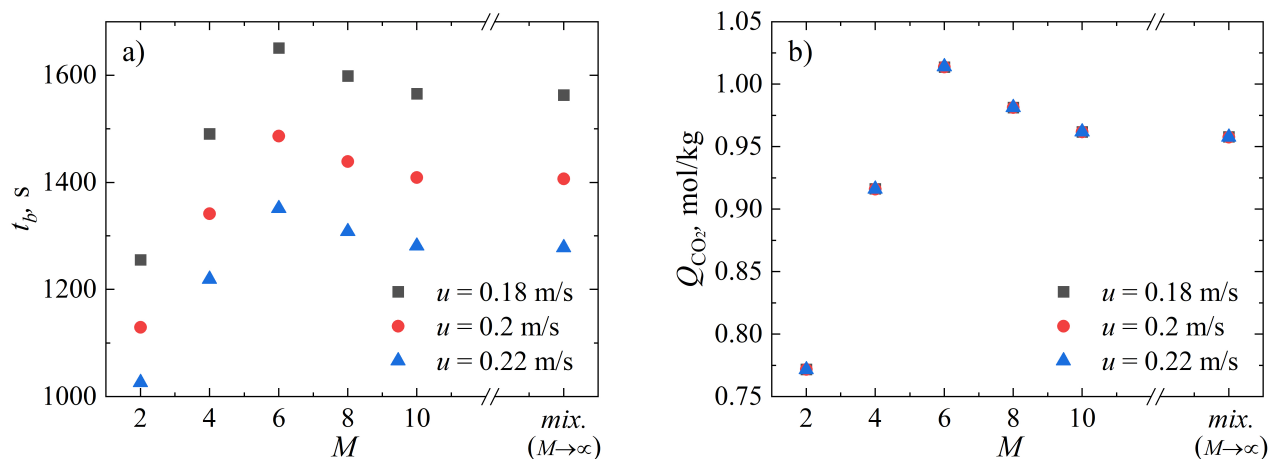


Figure 3. Breakthrough time,  $t_b$  (a) and corresponding values of average concentration of CO<sub>2</sub> in the solid phase,  $Q_{CO_2}$  (b) obtained for  $ads:cat = 2:1$ .

at the breakthrough determined from Eq. (18), obtained for different number of adsorbent and catalyst layers and for several values of superficial gas velocity, with a fixed value of adsorbent to catalyst ratio assumed to be 2:1. The last symbols (on the right) in both plots refer to the situation in which the bed is made of an uniform physical mixture of adsorbent and catalyst particles. Given the one-dimensional nature of the model, such intimate integration of two functionalities – sorptive and catalytic – in a hybrid reactor can also be interpreted as an infinite number of layers of particles, i.e.  $M \rightarrow \infty$ . On the other hand, a bed comprising two layers ( $M = 2$ ), i.e. one layer of adsorbent and a subsequent layer of catalyst, is basically a classic design of an adsorption column, except that the outlet zone contains an inert material with respect to adsorption process. The presence of this additional zone affects the residence time of the gas in the column (but not in the adsorbent itself) and the temperature of the gas at the outlet of the bed. As can be observed in Fig. 3, increasing the number of zones from 2 to 4, and then to 6, clearly improves the performance of the hybrid fixed bed both in terms of bed breakthrough time and the amount of CO<sub>2</sub> adsorbed by the time of breakthrough. Further increasing the number of zones leads to the reduction of the process performance, and at the same time is not justified in terms of process design or operation. An option when conducting cyclic adsorption and reactive regeneration processes is to supply or withdraw different amounts of heat to different zones or to keep selected sections of the apparatus under adiabatic conditions (Hussainy and Agar, 2016). This concept is technically more difficult to implement the higher the number of zones, the same applies, for example, to the replacement of part of the bed material.

Considering that the methanation process, which potentially might be carried out in the analyzed hybrid bed as the second step of the adsorption-reaction cycle, is highly exothermic and according to numerous studies the ideal H<sub>2</sub>:CO<sub>2</sub> molar ratio for the Sabatier is 4:1 (Schmider et al., 2021), in

the next step, the effect of the adsorbent to catalyst ratio,  $ads:cat$ , onto  $t_b$  and  $Q_{CO_2}$  was analyzed. It should be recalled here that in the case of CO<sub>2</sub> sequestration and subsequent methanation process, the adsorbent plays the role of a mass source of one of the reactants at the stage of the chemical reaction. For this kind of process, the highly exothermic nature of the reaction, combined with an improper choice of the ratio of adsorbent to catalyst, can cause excessive heat-up of the sorption zone, which may transfer into too rapid release of the adsorbed substance from solid (Jarczewski et al., 2022). This can result in a deficiency of the second reactant supplied in the gas stream (in case of methanation H<sub>2</sub>), and therefore incomplete conversion of the reactant being desorbed (here CO<sub>2</sub>). The selection of an optimal bed structure is therefore a complex multicriteria optimization problem, which ultimately should be analyzed for the entire process cycle. Nevertheless, it is also worthwhile to analyze how the ratio of the shares of the various functionalities in the bed affects the operation of the hybrid fixed bed already during the first step of the process. The results of such numerical simulations performed for  $M = 4$ ,  $M = 6$  and  $M \rightarrow \infty$  (i.e. for uniform mixture of particles) and different values of  $ads:cat$  are presented in Fig. 4.

It can be observed that in all cases evaluated via numerical simulations, the bed consisting of 6 layers performs best again. For all bed arrangements, increasing the ratio of adsorbent to catalyst, naturally yields an extension of the breakthrough time (Fig. 4a) and an increase in the average value of the concentration of CO<sub>2</sub> adsorbed in the bed at the time of breakthrough (Fig. 4b). However, this gain is noticeably weaker for higher values of this ratio, that is starting from  $ads:cat = 3:1$ . An increase in this ratio enhances the amount of heat released in the bed during adsorption, and thus contributes to an increase in bed temperature. For example, for a mixed arrangement, the average temperature of the bed at the time of breakthrough equals 317.26 K and 331.56 K, respectively, for  $ads:cat = 1:1$  and  $ads:cat = 6:1$ . Isotherms

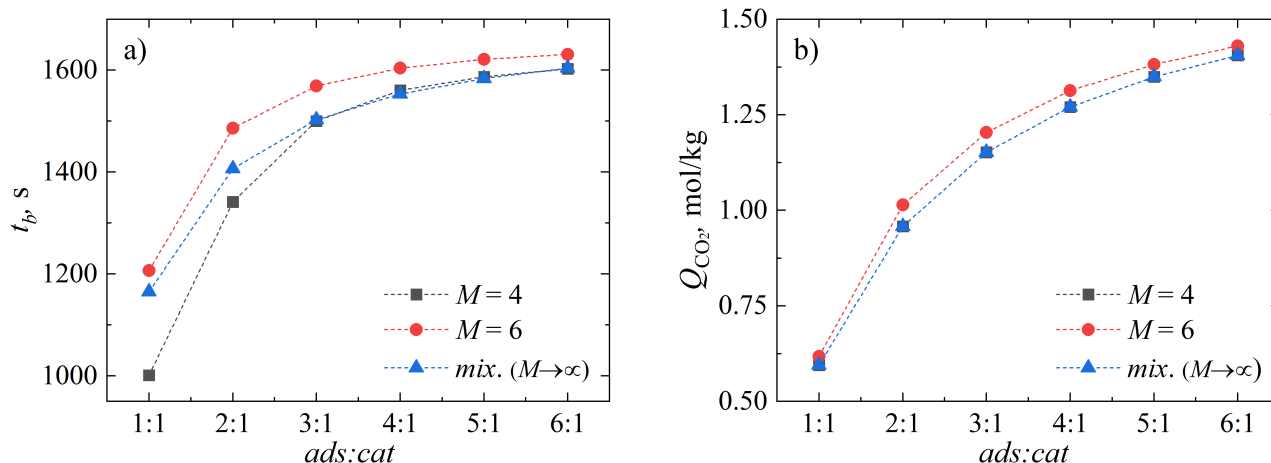


Figure 4. Breakthrough time,  $t_b$  (a) and corresponding values of average concentration of CO<sub>2</sub> in the solid phase,  $Q_{CO_2}$  (b) obtained for  $u = 0.2$  m/s.

of CO<sub>2</sub> adsorption on zeolite 13X (Fig. 2b) indicate that for the adopted process conditions and under equilibrium conditions, even such a small increase in temperature already reduces the sorption capacity by about 25%.

### 3.2. Assessment of the effect of thermal waves on the adsorption process

To provide an explanation of the trends described in the previous subsection and of the impact of temperature distributions in hybrid beds and, in particular, the thermal waves forming within the bed, on the adsorption process, representative temperature and CO<sub>2</sub> concentration profiles in the solid phase are shown in Figs. 5 and 6. Figure 5 compares the results obtained for an apparatus in which the bed consists of a uniform mixture of particles (Figs. 5a and 5c) and the bed consisting of two layers of adsorbent and two layers of catalyst (Figs. 5b and 5d). In the case of physical mixture of adsorbent and catalyst, which can be viewed as an adsorption column with a diluted bed of adsorbent, one can observe classical temperature waves forming and traveling through the bed (Fig. 5a), with the middle zone attaining constant temperature (Pan and Basmadjian, 1967). The wave shape is directly reflected in the adsorbate concentration patterns in the bed (Fig. 5c). Such dilution of the bed by the addition of catalyst (or inert) acts here locally, in the immediate vicinity of the sorbent particles. For layered arrangement of different functionalities, the catalyst sandwiched between the adsorbent (Fig. 2a) also acts as a heat sink. However, in this case the cooling effect is concentrated in the sections of the column filled with catalyst (inert) and is the source of the formation of characteristic temperature waves with multiple temperature extremes (Fig. 5b).

The uniform mixture of particles results to be superior to the 4-layer bed in terms of breakthrough time and average concentration of CO<sub>2</sub> adsorbed until breakthrough

( $t_b = 1341.6$  s and  $Q_{CO_2} = 0.916$  mol/kg obtained for  $M = 4$  versus  $t_b = 1406.4$  s and  $Q_{CO_2} = 0.9578$  mol/kg obtained for  $M \rightarrow \infty$ ). However, as previously observed (Fig. 3), increasing the number of layers to 6, makes the sectional rather than local heat removal from the flowing gas become more effective. This is connected with the fact that for  $M = 6$  ( $t_b = 1486.1$  s and  $Q_{CO_2} = 1.014$  mol/kg) non-monotonic concentration distributions of adsorbate in the solid phase are developed along the bed (Fig. 6b). Relatively low solid phase concentration of CO<sub>2</sub> at breakthrough obtained for  $M = 6$  in the first portion of the second adsorbent layer (dashed line, in correspondence to  $x = 0.33$  m in Fig. 6b) is associated with the first peak of the temperature profile (Fig. 6a). The catalyst layers sandwiched between the adsorbent in the initial phase of the adsorption cycle bring about a significant cooling of the gas before entering the next sorbent layer. The traveling of such thermal waves over time causes that, for instance for  $M = 6$ , at the inlet of the second zone and in the correspondence of the breakthrough time there are much higher temperatures than at its center (dashed line in Fig. 6a, values of  $T$  in correspondence of  $x = 0.33$  m and e.g.  $x = 0.5$ ).

### 3.3. Analysis of the impact of effective thermal conductivity on the adsorption process

The observations made in the previous section suggest that another important element in the analysis of the performance of layered beds is the mechanism of heat transport. Therefore, considering additionally discrepancies as large as one order of magnitude in various correlations for calculating effective axial conductivity (Díaz-Heras et al., 2020), the final step of this study involved analyzing the effect of  $K_{ax}$  on the evolution of bed temperature and gas and solid phase CO<sub>2</sub> concentration. Nevertheless, it must be emphasized here that the choice for the calculation of the correlation authored by Kunii and Smith (1960) was motivated by the fact that for

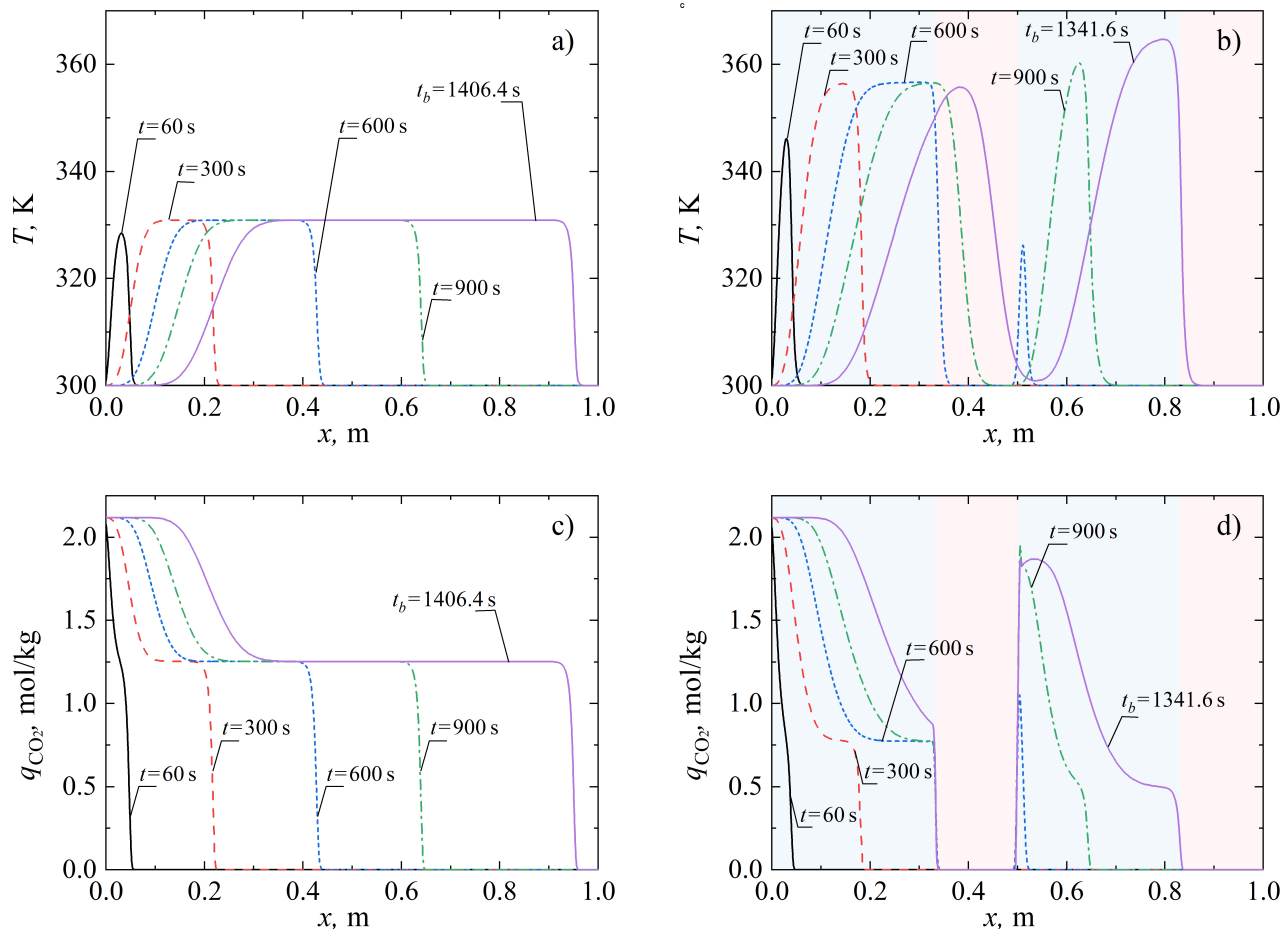


Figure 5. Temperature profiles along the fixed bed composed of a uniform physical mixture of particles (a) and along layered bed (b), and corresponding values of solid phase concentration of CO<sub>2</sub>: bed made of physical mixture of particles (c) and layered bed with  $M = 4$  (d) obtained for  $ads:cat = 2:1$  and  $u = 0.2$  m/s.

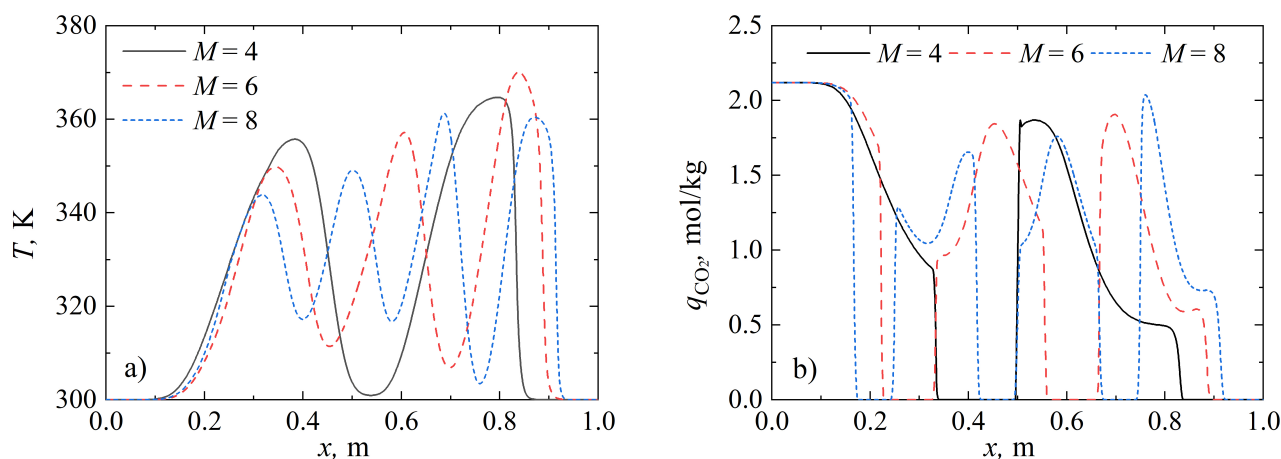


Figure 6. Temperature profiles along the layered bed (a) and corresponding values of solid phase concentration of CO<sub>2</sub> (b) corresponding to  $t_b$  and obtained for  $ads:cat = 2:1$  and  $u = 0.2$  m/s.

the values of parameter  $\kappa$  which was of the order of 10, this correlation provides the values of effective thermal conductivity consistent with experimental results (van Antwerpen et al., 2010).

Figure 7 shows the temperature profiles along the bed at breakthrough time and the corresponding solid phase concentration of carbon dioxide profiles determined for  $M = 6$ . These results were obtained by determining the effective ax-

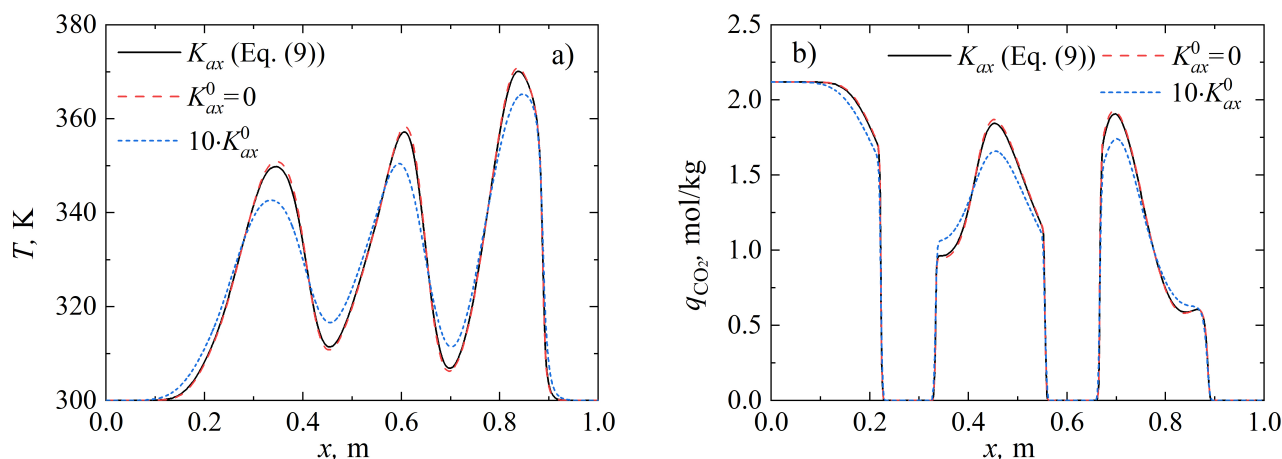


Figure 7. Temperature profiles along the layered bed with  $M = 6$  (a) and corresponding values of solid phase concentration of  $\text{CO}_2$  (b) corresponding to  $t_b$  and obtained for  $ads:cat = 2:1$  and  $u = 0.2$  m/s. Solid line – solution determined with  $K_{ax}$  calculated according to Eq. (9), dashed line – solution determined with neglected static effective thermal conductivity,  $K_{ax}^0$ , dotted line – solution determined with  $K_{ax}$  increased by factor 10.

ial thermal conductivity of the bed, respectively: (a) using formula given by Eq. (9); (b) neglecting the static effective axial thermal conductivity in this formula, i.e. assuming that  $K_{ax}^0 = 0$ ; (c) multiplying the static effective axial conductivity by a factor of 10. It can be observed in Fig. 7 that neglecting the static effective axial conductivity has very little quantitative and qualitative effect on the temperature and concentration distributions. However, multiplying the originally determined from Eq. (10) value of  $K_{ax}^0$  by 10, which corresponds to reduction of the characteristic time of conduction by factor 10, clearly affects the temperature and  $\text{CO}_2$  concentration distributions along the column. Despite significantly lower maximum temperatures (Fig. 7a), the higher value of the effective axial thermal conductivity unfavorably affects the concentration of adsorbate in the sorbent (Fig. 7b). Lower temperature gradients in the vicinity of peaks located around the boundary of the catalyst and adsorbent layers contribute to higher average tempera-

ture values of the initial parts of successive adsorbent layers. These results confirm that the correct prediction of the adsorption process behavior requires the careful selection of experimental correlation for determination of  $K_{ax}$  (Díaz-Heras et al., 2020). Moreover, they indicate that thermal conductivity of the material constituting the heat sink in a hybrid bed might be an additional optimization (design) variable of the system. While the thermal conductivity of the catalyst can not be arbitrarily chosen and is rather high for nickel or ruthenium catalysts, one way to reduce the contribution of conductive heat transport could be to dilute the catalytic zone using a material characterized by lower thermal conductivity.

The phenomenon described above is analogous to the effect of dispersion on the adsorption process, which is reflected in the bed breakthrough curves reported in Fig. 8a. The higher the value of  $K_{ax}^0$  and thus  $K_{ax}$ , the lower the bed break-

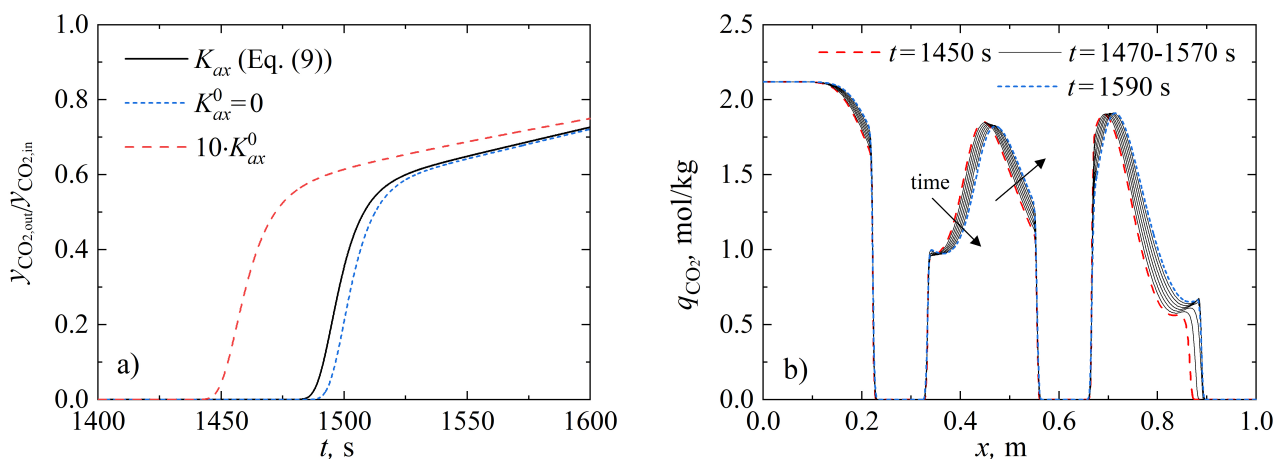


Figure 8. Temporal evolution of  $y_{\text{CO}_2,\text{out}}/y_{\text{CO}_2,\text{in}}$  for the layered bed with  $M = 6$  (a) and representative temperature profiles along the bed for  $K_{ax}$  calculated according to Eq. (9) (b) obtained for  $ads:cat = 2:1$  and  $u = 0.2$  m/s.

through time. The somewhat atypical shape of the breakthrough curves (i.e. a rather rapid increase in the concentration ratio from a value corresponding to the break point to about 0.6, followed by a very slow increase in this ratio toward a value corresponding to the exhaustion of the bed) is the result of simultaneous adsorption and desorption phenomena taking place in the hybrid bed, and resulting from the oscillatory nature of the thermal waves. Figure 8b illustrates the solid phase concentration of CO<sub>2</sub> along the bed obtained for the case in which  $K_{ax}$  was not modified (i.e. value calculated based on Eq. (9)) and plotted for time instants in the neighborhood of the breakthrough time (for the case considered here  $t_b = 1486.1$  s). The behavior of the profiles over time in the second and third adsorbent layers indicates that shortly before the bed breakthrough, the adsorbate concentration begins to decrease at the entrance to these zones i.e. desorption begins to occur here. This is due to the non-monotonic temperature wave traveling through the column. At the same time, in the downstream parts of the adsorbent layers, where temperatures are still relatively low (Fig. 7b), re-adsorption occurs. The occurrence of the competitive phenomenon of desorption and adsorption implies that the bed saturation time after the breakthrough is expected to be significantly longer for a layered bed than for a conventional bed.

## 4. CONCLUSIONS

A mathematical model of a non-isothermal, layered fixed-bed for carbon dioxide capture was developed and solved numerically to demonstrate the possibility of manipulating process performance by structuring the bed. The performance of the hybrid bed, assessed in terms of breakthrough time and average concentration of carbon dioxide in the solid phase corresponding to the breakthrough time, was assessed for different numbers of layers and adsorbent to catalyst ratios. The results obtained for the layered bed were then compared with those obtained for a column packed with a uniform mixture of adsorbent and catalyst particles, considered as inert for the adsorption process examined here exclusively.

In general, a baseline 2-layer bed (one layer for the adsorbent and one for the catalyst) can be regarded as a classical adsorption column, with an additional exit zone being inert with respect to the adsorption process. The results obtained for a larger number of zones confirm that such multilayer systems outperform the baseline, with the best performance observed for  $M = 6$ . Nevertheless, continued increase in the number of layers ( $M > 6$ ) did not further improve the process performance, as both the breakthrough time and the average concentration of adsorbed CO<sub>2</sub> tended to decline again. Anyhow, despite this deterioration in performance as  $M$  increased, both the multilayer and the physical mixture of the two types of particles (i.e.  $M \rightarrow \infty$ ) still proved to be better than the baseline 2-layer hybrid bed.

Particular attention was paid in the study to temperature distributions along the bed and how they affect CO<sub>2</sub> concentration profiles and breakthrough times. It is worth mentioning here the formation of atypical thermal waves with multiple temperature extremes, resulting from the presence of a catalyst acting as a heat sink in the hybrid layered bed. They differ significantly from the thermal waves arising in a bed packed with a physical mixture of adsorbent and catalyst or a classical adsorption column, and can induce a complex process of desorption and re-adsorption in the bed.

The results suggest that proper tailoring of the bed might be an excellent tool for controlling temperature profiles and, consequently, the performance of the apparatus and thus its optimization. It is expected that an appropriate bed structure will also allow to control temperature profiles along the bed, and thus CO<sub>2</sub> desorption, at the following methanation stage, where management of the heat needed to desorb CO<sub>2</sub> from the solid and that released by exothermic reaction of its hydrogenation to methane is also essential. Due to the cyclic nature of the entire process, the complexity of the involved phenomena, as well as different goals – both of a technological, energetic and economic nature – the optimization problem should be approached using multicriteria optimization tools, such as Pareto analysis. These aspects are the subject of current and future research, and they will be further extended to the two-dimensional model of the bed in order to account for radial mass and heat transport phenomena.

## ACKNOWLEDGEMENTS

*The research was financed by the Polish National Science Centre, under research project "Experimental and numerical analysis of mass and heat transport in "tailor-made" fixed beds for gas-solid processes", no. UMO-2021/42/E/ST8/00313.*

## SYMBOLS

$a, a_0$	parameters of the Toth isotherm (Eq. (4) and (5)), mol/(kg·kPa)
$A$	slope of the sigmoid (Eq. (17)), –
$b, b_0$	parameters of the Toth isotherm (Eq. (4) and (5)), 1/kPa
$c$	parameter of the Toth model (Eq. (4) and (5)), K
$c_{ads}$	heat capacity of the adsorbate phase, J/(kg·K)
$c_g$	heat capacity of the gas, J/(kg·K)
$c_s$	heat capacity of the solid, J/(kg·K)
$C_{f,CO_2}$	molar gas phase concentration of CO <sub>2</sub> in the feed, mol/m <sup>3</sup>
$C_{CO_2}$	molar gas phase concentration of CO <sub>2</sub> , mol/m <sup>3</sup>
$D_{ax}$	axial dispersion coefficient, m <sup>2</sup> /s
$D_e$	effective diffusivity, m <sup>2</sup> /s
$D_K$	Knudsen diffusivity, m <sup>2</sup> /s
$D_m$	molecular diffusivity, m <sup>2</sup> /s
$E$	parameter of the Toth isotherm (Eq. (4) and (5)), K

$f_{\text{ads}}$	volume fraction of adsorbent particles in the bed, –
$f_{\text{cat}}$	volume fraction of catalyst particles in the bed, –
$\Delta H_{\text{ads}}$	isosteric enthalpy of adsorption of CO <sub>2</sub> , J/mol
$k$	LDF mass transfer coefficient, 1/s
$K_{\text{ax}}$	effective axial thermal conductivity of the packed bed, W/(m·K)
$K_{\text{ax}}^0$	static effective thermal conductivity of the packed bed, W/(m·K)
$L$	length of the bed, m
$M$	total number of adsorbent and catalyst particles layers in the column, –
$n_j$	number of contact points on a semispherical surface of one solid particle (Eq. (13)), –
$N$	number of discretization nodes, –
$p$	total pressure, Pa
$p_{\text{CO}_2}$	partial pressure of CO <sub>2</sub> (Eqs. (4) and (8)), kPa
$q_{\text{CO}_2}$	solid phase concentration of CO <sub>2</sub> , mol/kg
$q_{\text{CO}_2}^*$	equilibrium solid phase concentration of CO <sub>2</sub> , mol/kg
$Q_{\text{CO}_2}$	average solid phase concentration of CO <sub>2</sub> within the bed corresponding to breakthrough time, mol/kg
$r_p$	particle radius, m
$R$	universal gas constant, J/(mol·K)
$t$	time, s
$t_b$	breakthrough time, s
$T$	temperature, K
$T_0$	initial temperature of the bed, K
$T_f$	feed gas temperature, K
$u$	superficial gas velocity, m/s
$y$	molar fraction of component $i$ , –
$x$	longitudinal coordinate in the reactor, ;m

#### Greek symbols

$\gamma$	parameter of the experimental correlation (Eq. (10)–(12)) for determination of the static effective thermal conductivity of the packed bed, –
$\varepsilon_b$	voidage of the bed, –
$\varepsilon_p$	particle porosity, –
$\varepsilon_t$	total voidage of the bed, –
$\theta$	angle corresponding to gas film near one contact point points between particles within the bed (Eq. (12)), radians
$\kappa$	thermal conductivity ratio, –
$\lambda_g$	gas phase thermal conductivity, W/(m·K)
$\lambda_s$	solid phase thermal conductivity, W/(m·K)
$\rho_b$	bulk density of the bed, kg/m <sup>3</sup>
$\rho_g$	gas density, kg/m <sup>3</sup>
$\tau, \tau_0$	parameters of the Toth isotherm (Eqs. (4) and (5)), –
$\tau_p$	tortuosity factor, –
$\psi_j, \psi_t$	parameters of the experimental correlation (Eqs. (10)–(12)) for determination of the static effective thermal conductivity of the packed bed, –

#### Subscripts

ads	adsorbent or adsorbate
cat	catalyst
in	inlet
out	outlet

## REFERENCES

- Agar D.W., 2005. The dos and don'ts of adsorptive reactors, In: Sundmacher K., Kienle A., Seidel-Morgenstern A. (Eds.), *Integrated chemical processes: Synthesis, operation, analysis, and control*. WILEY-VCH Verlag GmbH & Co. KGaA, Weinheim, 203–232. DOI: [10.1002/3527605738.ch7](https://doi.org/10.1002/3527605738.ch7).
- Al-Janabi N., Vakili R., Kalumpasut P., Gorgojo P., Siperstein F.R., Fan X., 2018. Velocity variation effect in fixed bed columns: A case study of CO<sub>2</sub> capture using porous solid adsorbents. *AIChE J.*, 64, 2189–2197. DOI: [10.1002/aic.16135](https://doi.org/10.1002/aic.16135).
- Bremer J., Rätze K.H.G., Sundmacher K., 2017. CO<sub>2</sub> methanation: Optimal start-up control of a fixed-bed reactor for power-to-gas applications. *AIChE J.*, 63, 23–31. DOI: [10.1002/aic.15496](https://doi.org/10.1002/aic.15496).
- Chao C., Deng Y., Dewil R., Baeyens J., Fan X., 2021. Post-combustion carbon capture. *Renewable Sustainable Energy Rev.*, 138, 110490. DOI: [10.1016/j.rser.2020.110490](https://doi.org/10.1016/j.rser.2020.110490).
- Choi W.-K., Kwon T.-I., Yeo Y.-K., Lee H., Song H.K., Na B.-K., 2003. Optimal operation of the pressure swing adsorption (PSA) process for CO<sub>2</sub> recovery. *Korean J. Chem. Eng.*, 20, 617–623. DOI: [10.1007/BF02706897](https://doi.org/10.1007/BF02706897).
- Dhoke C., Zaabout A., Cloete S., Amini S., 2021. Review on reactor configurations for adsorption-based CO<sub>2</sub> capture. *Ind. Eng. Chem. Res.*, 60, 3779–3798. DOI: [10.1021/acs.iecr.0c04547](https://doi.org/10.1021/acs.iecr.0c04547).
- Díaz-Heras M., Belmonte J.F., Almendros-Ibáñez J.A., 2020. Effective thermal conductivities in packed beds: Review of correlations and its influence on system performance. *Appl. Therm. Eng.*, 171, 115048. DOI: [10.1016/j.applthermaleng.2020.115048](https://doi.org/10.1016/j.applthermaleng.2020.115048).
- Ding Y., Alpay E., 2000. Equilibria and kinetics of CO<sub>2</sub> adsorption on hydrotalcite adsorbent. *Chem. Eng. Sci.*, 55, 3461–3474. DOI: [10.1016/S0009-2509\(99\)00596-5](https://doi.org/10.1016/S0009-2509(99)00596-5).
- Do D.D., 1998. *Adsorption analysis: Equilibria and kinetics*. Imperial College Press, London. DOI: [10.1142/p111](https://doi.org/10.1142/p111).
- Harlick P.J.E., Tezel F.H., 2004. An experimental adsorbent screening study for CO<sub>2</sub> removal from N<sub>2</sub>. *Microporous Mesoporous Mater.*, 76, 71–79. DOI: [10.1016/j.micromeso.2004.07.035](https://doi.org/10.1016/j.micromeso.2004.07.035).
- Hira U., Kamal A., Tahir J., 2023. Chapter 11 – Industrial carbon dioxide capture and utilization, In: Inamuddin, Altalhi T. (Eds.), *Green Sustainable Process for Chemical and Environmental Engineering and Science*. Elsevier, Amsterdam, 231–278. DOI: [10.1016/B978-0-323-99429-3.00023-0](https://doi.org/10.1016/B978-0-323-99429-3.00023-0).
- Hussainy M., Agar D.W., 2016. Structural and operational optimality of adsorptive reactors. *Chem. Eng. Technol.*, 11, 2135–2141. DOI: [10.1002/ceat.201600197](https://doi.org/10.1002/ceat.201600197).
- Hussainy M., Agar D.W., 2018. Modeling and optimization of the cyclic steady state operation of adsorptive reactors. *Chin. J. Chem. Eng.*, 26, 1321–1329. DOI: [10.1016/j.cjche.2018.04.013](https://doi.org/10.1016/j.cjche.2018.04.013).
- Jarczewski S., Barańska K., Drozdek M., Michalik M., Bizon K., Kuśtrowski P., 2022. Energy-balanced and effective adsorption-catalytic multilayer bed system for removal of volatile organic compounds. *Chem. Eng. J.*, 431, 133388. DOI: [10.1016/j.cej.2021.133388](https://doi.org/10.1016/j.cej.2021.133388).

- Jo S., Lee J.H., Kim T.Y., Woo J.H., Ryu H.-J., Hwang B., Lee S.C., Kim J.C., Gilliard-AbdulAziz K.L., 2022. A fundamental study of CO<sub>2</sub> capture and CH<sub>4</sub> production in a rapid cyclic system using nickel-lithium-silicate as a catal-sorbent. *Fuel*, 311, 122602. DOI: [10.1016/j.fuel.2021.122602](https://doi.org/10.1016/j.fuel.2021.122602).
- Kaguei S., Shemilt L.W., Wakao N., 1989. Models and experiments on adsorption columns with constant wall temperature – radially varying and radially lumped models. *Chem. Eng. Sci.*, 44, 483–491. DOI: [10.1016/0009-2509\(89\)85026-2](https://doi.org/10.1016/0009-2509(89)85026-2).
- Ko D., Siriwardane R., Biegler L.T., 2003. Optimization of a pressure-swing adsorption process using zeolite 13X for CO<sub>2</sub> for sequestration. *Ind. Eng. Chem. Res.*, 42, 339–348. DOI: [10.1021/ie0204540](https://doi.org/10.1021/ie0204540).
- Kunii D., Smith J.M., 1960. Heat transfer characteristics of porous rocks. *AIChE J.*, 6, 71–78. DOI: [10.1002/aic.690060115](https://doi.org/10.1002/aic.690060115).
- Maina J.W., Pringle J.M., Razal J.M., Nunes S., Vega L., Gallucci F., Dum e L.F., 2021. Strategies for integrated capture and conversion of CO<sub>2</sub> from dilute flue gases and the atmosphere. *ChemSusChem*, 14, 1805–1820. DOI: [10.1002/cssc.202100010](https://doi.org/10.1002/cssc.202100010).
- Martins V.F.D., Miguel C.V., Gonalves J.C., Rodrigues A.E., Madeira L.M., 2022. Modeling of a cyclic sorption–desorption unit for continuous high temperature CO<sub>2</sub> capture from flue gas. *Chem. Eng. J.*, 434, 134704. DOI: [10.1016/j.cej.2022.134704](https://doi.org/10.1016/j.cej.2022.134704).
- Masson-Delmotte V., Zhai P., P ortner H.O., Roberts D., Skea J., Shukla P.R., et al., 2018. Global warming of 1.5  C, 1. An IPCC Special Report on the Impacts of Global Warming.
- Miguel C.V., Soria M.A., Mendes A., Madeira L.M., 2017. A sorptive reactor for CO<sub>2</sub> capture and conversion to renewable methane. *Chem Eng. J.*, 322, 590–602. DOI: [10.1016/j.cej.2017.04.024](https://doi.org/10.1016/j.cej.2017.04.024).
- Moioli E., 2022. Process intensification and energy transition: A necessary coupling? *Chem. Eng. Process. Process Intensif.*, 179, 109097. DOI: [10.1016/j.cep.2022.109097](https://doi.org/10.1016/j.cep.2022.109097).
- Moioli E., Z uttel A., 2020. A model-based comparison of Ru and Ni catalysts for the Sabatier reaction. *Sustainable Energy Fuels*, 4, 1396–1408. DOI: [10.1039/C9SE00787C](https://doi.org/10.1039/C9SE00787C).
- Pan C.Y., Basmadjian D., 1967. Constant-pattern adiabatic fixed-bed adsorption. *Chem. Eng. Sci.*, 22, 285–297. DOI: [10.1016/0009-2509\(67\)80115-5](https://doi.org/10.1016/0009-2509(67)80115-5).
- Pan C.Y., Basmadjian D., 1970. An analysis of adiabatic sorption of single solutes in fixed beds: pure thermal wave formation and its practical implications. *Chem. Eng. Sci.*, 25, 1653–1664. DOI: [10.1016/0009-2509\(70\)80056-2](https://doi.org/10.1016/0009-2509(70)80056-2).
- Patra B.R., Gouda S.P., Pattnaik F., Nanda S., Dalai A.K., Naik S., 2022. Chapter 1 – A brief overview of recent advancements in CO<sub>2</sub> capture and valorization technologies, In: Nanda S., Vo D.-V.N., Nguen V.-H. (Eds.), *Carbon dioxide capture and conversion. Advanced materials and processes*. Elsevier, Amsterdam, 1–16. DOI: [10.1016/B978-0-323-85585-3.00011-0](https://doi.org/10.1016/B978-0-323-85585-3.00011-0).
- Poling B.E., Prausnitz J.M., O’Connell J.P., 2001. *Properties of gases and liquids*. 5<sup>th</sup> edition, McGraw-Hill Education, New York.
- Raghavan N.S., Ruthven D.M., 1984. Dynamic behaviour of an adiabatic adsorption column—II: Numerical simulation and analysis of experimental data. *Chem. Eng. Sci.*, 39, 1201–1212. DOI: [10.1016/0009-2509\(84\)85081-2](https://doi.org/10.1016/0009-2509(84)85081-2).
- Rezaei F., Grahn M., 2012. Thermal management of structured adsorbents in CO<sub>2</sub> capture processes. *Ind. Eng. Chem. Res.*, 51, 4025–4034. DOI: [10.1021/ie201057p](https://doi.org/10.1021/ie201057p).
- Rezaei F., Webley P., 2009. Optimum structured adsorbents for gas separation processes. *Chem. Eng. Sci.*, 64, 5182–5191. DOI: [10.1016/j.ces.2009.08.029](https://doi.org/10.1016/j.ces.2009.08.029).
- Schmider D., Maier L., Deutschmann O., 2021. Reaction kinetics of CO and CO<sub>2</sub> methanation over nickel. *Ind. Eng. Chem. Res.*, 60, 5792–5805. DOI: [10.1021/acs.iecr.1c00389](https://doi.org/10.1021/acs.iecr.1c00389).
- Shigaki N., Mogi Y., Haraoka T., Furuya E., 2020. Measurements and calculations of the equilibrium adsorption amounts of CO<sub>2</sub>–N<sub>2</sub>, CO–N<sub>2</sub>, and CO<sub>2</sub>–CO mixed gases on 13X zeolite. *SN Appl. Sci.*, 2, 488. DOI: [10.1007/s42452-020-2298-y](https://doi.org/10.1007/s42452-020-2298-y).
- Styring P., Duckworth E.L., Platt E.G., 2021. Synthetic fuels in a transport transition: fuels to prevent a transport underclass. *Front. Energy Res.*, 9, 707867. DOI: [10.3389/fenrg.2021.707867](https://doi.org/10.3389/fenrg.2021.707867).
- Thang H.V., Grajciar L., Nachtigall P., Bludsk y O., Are an C.O., Fr ydov a E., Bul anek R., 2014. Adsorption of CO<sub>2</sub> in FAU zeolites: Effect of zeolite composition. *Catal. Today*, 227, 50–56. DOI: [10.1016/j.cattod.2013.10.036](https://doi.org/10.1016/j.cattod.2013.10.036).
- van Antwerpen W., du Toit C.G., Rousseau P.G., 2010. A review of correlations to model the packing structure and effective thermal conductivity in packed beds of mono-sized spherical particles. *Nucl. Eng. Des.*, 240, 1803–1818. DOI: [10.1016/j.nucengdes.2010.03.009](https://doi.org/10.1016/j.nucengdes.2010.03.009).
- Wakao N., Funazkri T., 1978. Effect of fluid dispersion coefficients on particle-to-fluid mass transfer coefficients in packed beds: Correlation of Sherwood numbers. *Chem. Eng. Sci.*, 33, 1375–1384. DOI: [10.1016/0009-2509\(78\)85120-3](https://doi.org/10.1016/0009-2509(78)85120-3).
- Wang Y., LeVan M.D., 2009. Adsorption equilibrium of carbon dioxide and water vapor on zeolites 5A and 13X and silica gel: Pure components. *J. Chem. Eng. Data*, 54, 2839–2844. DOI: [10.1021/je800900a](https://doi.org/10.1021/je800900a).
- Yagi S., Kunii D., Wakao N., 1960. Studies on axial effective thermal conductivities in packed beds. *AIChE J.*, 6, 543–546. DOI: [10.1002/aic.690060407](https://doi.org/10.1002/aic.690060407).